Available online at www.sciencedirect.com

ScienceDirect

International Journal of Solids and Structures 43 (2006) 7644–7658

INTERNATIONAL JOURNAL OF SOLIDS and STRUCTURES

www.elsevier.com/locate/ijsolstr

A blast-tolerant sandwich plate design with a polyurea interlayer

Yehia A. Bahei-El-Din *, George J. Dvorak, Olivia J. Fredricksen

Department of Mechanical, Aerospace and Nuclear Engineering, Rensselaer Polytechnic Institute, 110 8th Street, Troy, NY 12180-3590, USA

Received 10 August 2005; received in revised form 12 February 2006
Available online 28 March 2006

Abstract

This paper presents a study of both conventional and modified sandwich plate designs subjected to blast loads. The conventional sandwich Design (1) consists of thin outer (loaded side) and inner facesheets made of fibrous laminates, separated by a layer of structural foam core. In the modified Design (2), a thin polyurea interlayer is inserted between the outer facesheet and the foam core. Comparisons of the two designs are made during a long time period of 5.0 ms, initiated by a pressure impulse lasting 0.05 ms applied to a single span of a continuous plate. In the initial response period the overall deflections are limited and significant foam core crushing is caused in the conventional design by the incident compression wave. This type of damage is much reduced in the modified design, by stiffening of the polyurea interlayer under shock compression, which provides support to the outer facesheet and alters propagation of stress waves into the foam core. This benefits the long term, bending response and leads to significant reductions in facesheet strains and overall deflection. The total kinetic energy of the modified sandwich plate is much lower than that of a conventionally designed plate, and so is the stored and dissipated strain energy. Similar reductions are found when the conventional and the enhanced sandwich plates have equal overall thickness or equal total mass.

Keywords: Sandwich plates; Blast load; Interlayers; Polyurea; Finite elements

1. Introduction

While the response of sandwich plates to dynamic loads in general has received attention only recently, monolithic plates have been studied extensively over several decades. In particular, the behavior of metallic plates under blast loads was investigated in theoretical as well as numerical studies. The theoretical formulations idealized blast loads as either zero-period or rectangular, uniformly distributed pressure impulses, and were often accompanied by simplified constitutive laws. Theoretical formulations for the response of rigid-plastic circular plates with clamped supports are given by Wang and Hopkins (1954) for a zero-period impulse and by Florence (1966) for a rectangular impulse. In their work, bending kinematics was assumed to be linear, and membrane stretching was neglected. On the other hand, Symonds and Wierzbicki (1979) considered the

* Corresponding author. Tel.: +1 518 276 2776; fax: +1 518 276 6025.
E-mail address: baheiy@rpi.edu (Y.A. Bahei-El-Din).

0020-7683/$ - see front matter
doi:10.1016/j.ijsolstr.2006.03.021

same plate geometry and load but neglected bending and examined the finite displacement response under in-plane stretching. Finite deformations were included in the formulation for the bending of circular, monolithic plates by Jones (1971). An extensive review of the literature on monolithic plates subjected to impact is also given by Jones (1989).

Numerical solutions for monolithic as well as sandwich plates subjected to dynamic loads can generally be obtained through the finite element method. This permits analysis of more complex plate geometries and boundary conditions, and consideration of a variety of material behaviors and load histories. So far, finite element solutions of sandwich plates subjected to blast loading have been obtained for simple geometries and boundary conditions, such as clamped circular plates, and uniform pressure impulses (Xue and Hutchinson, 2003, 2004; Qui et al., 2003). These studies advanced understanding of the different responses of sandwich and monolithic plates, and evaluated the effect of the core geometry on the overall response. Both geometric and material nonlinearities caused by plastic deformation of metallic cores and crushing of foam cores were modeled, but local delamination was not considered.

Theoretical solutions for sandwich plates subjected to blast loads are rare. Taylor (1963) provides a one-dimensional analysis for the dynamic response of a sandwich plate subjected to an exponential blast wave. This solution was adopted by Fleck and Deshpande (2004) to describe the first of a three-stage solution of a clamped sandwich beam subjected to blast loading prior to crushing of the core and bending of the beam. While the core crushing stage of the deformation was also treated as one-dimensional, the third stage combined bending and stretching to determine the dynamic structural response of the sandwich beam.

The present work is concerned with evaluation of certain modified sandwich plate designs, which offer resistance to blast loads far superior to that of conventional designs consisting of stiff laminated AS4/3501-6 carbon/epoxy composite facesheets and a compliant and crushable Divinycell H100 structural foam core. In an apparently single effort to improve structural performance and damage resistance of sandwich structures under the said loads, Dvorak and Suvorov (2006) introduced polyurethane and elastomeric foam interlayers under the outer, loaded facesheet. These interlayers offer support to the facesheet and at the same time protect the foam core from excessive deformation and crushing. Remarkably significant improvement in impact damage resistance of the modified designs has been demonstrated by Dvorak and Suvorov (2006) and Suvorov and Dvorak (2005a,b).

Recent high velocity impact experiments performed on polyurea elastomers (Yi and Boyce, 2004; Clifton and Jiao, 2004; Nemat-Nasser, 2004) revealed a significant stiffening behavior under high strain rates. The modified design examined in the present work employs a thin polyurea interlayer inserted between the outer facesheet and the foam core. Under the incident compression wave caused by the blast load, this interlayer stiffens gradually and shields the foam core.

Explicit finite element analysis of the sandwich plates is applied to evaluate the local fields and overall response in conventional and modified, multi-span sandwich plates. The blast load is applied uniformly to a single span as an exponentially decaying pressure impulse which lasts 0.05 ms. Response of the plate is investigated far beyond this period up to 5 ms. Sandwich designs considered in this investigation are described in Section 2 together with material properties, geometry and loads. Finite element models employed in analysis of continuous sandwich plates are described in Section 3 and the results are presented in Section 4. Finally discussion and conclusions of this work are given in Section 5.

2. Sandwich designs, material properties and loads

A multi-span sandwich panel supported by equally spaced rigid stiffeners is considered. The length of a single span between supports is $L = 1000$ mm, and the total thickness $h = 57.2$ mm, Fig. 1. The total width, measured in the X_2-direction of Fig. 1 is assumed to be sufficiently large, so that the plate can be analyzed in plane strain, with displacements $u_2 = 0$ everywhere. Width of the supporting stiffeners is $d = 100$ mm, such that the clear span of the sandwich plate is $L - d = 900$ mm.

Two structural arrangements of the plate are analyzed, both of a total thickness $h = 57.2$ mm, Fig. 2. In the conventional Design (1), the laminated composite facesheets are bonded to a structural foam core, to form a symmetric sandwich cross-section. Each of the facesheets is $h_f = 3.6$ mm thick, while the foam core thickness is equal to $h_c = 50$ mm. Modified Design (2) features a thin polyurea interlayer that is inserted between the outer

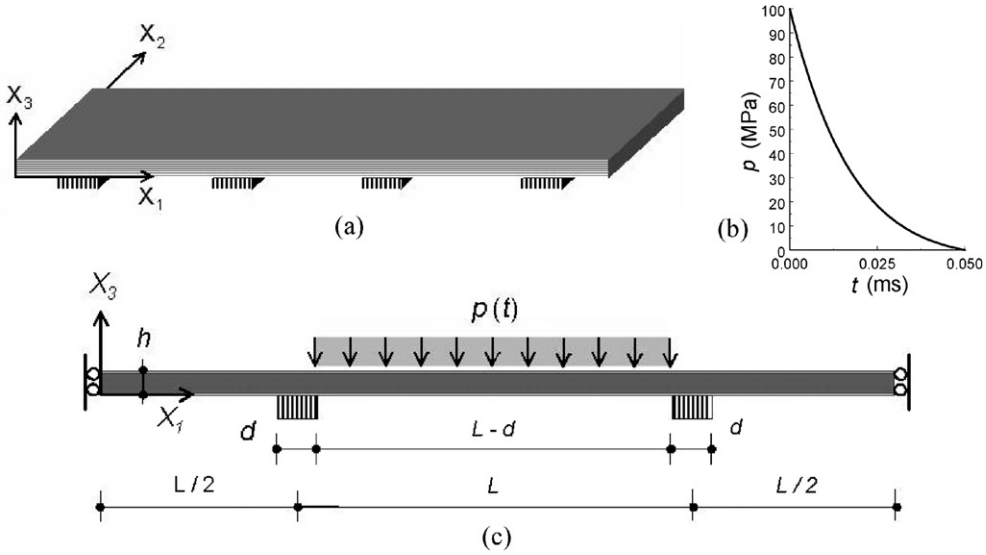

Fig. 1. Geometry and loading of a continuous sandwich plate.

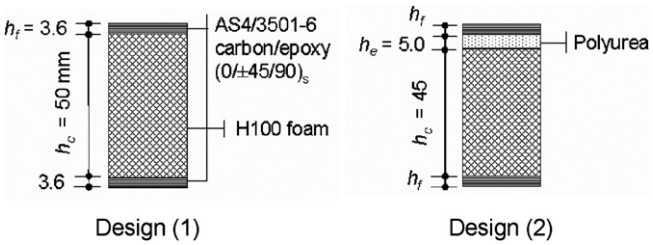

Fig. 2. Cross-sections of conventional and modified designs of sandwich plates.

facesheet and foam core. The thickness of the interlayer was selected as $h_e = 5.0$ mm and the total foam core thickness was reduced to $h_c - h_e = 45$ mm. Specific material properties of the facesheet laminates, polyurea interlayer and foam core, listed in Tables 1 and 2, are derived from the following material models provided by the LS-Dyna finite element code (LSTC, 2003).

Table 1
Elastic properties and dimensions of sandwich plate constituents

Property (units)	$(0/\pm45/90)_s$ AS4/3501-6 carbon/epoxy	H100 Divinycell foam	Polyurea
Material type	Orthotropic, elastic	Isotropic, crushable	Isotropic, elastic–plastic–hydrodynamic
LS-Dyna material #	2	63	10
$E_1 = E_2$ (GPa)	55.022	0.111	2.52
E_3 (GPa)	10.792	0.111	2.52
G_{12} (GPa)	21.319	0.050	0.86
$G_{13} = G_{23}$ (GPa)	4.953	0.050	0.86
ν_{12}	0.29	0.1	0.465
$\nu_{13} = \nu_{23}$	0.248	0.1	0.465
ρ_0 (kg/m^3)	1580	100	1070
Compressive yield strength (MPa)	–	1.7	10.0
Thickness (mm)			
Design (1) (mass = 16.38 kg/m^2)	3.6	50.0	–
Design (2) (mass = 21.23 kg/m^2)	3.6	45.0	5.0

Table 2
Plasticity and equation of state (EOS) parameters for polyurea

Model	Reference equation	Parameters
Plasticity	(1)	$\sigma_y^0 = 10$ MPa, $E_h = 10$ MPa, $a_1 = 2.0$, $a_2 = 0$
Gruneisen's EOS	(2)	$C = 25$ m/s, $\gamma_0 = 1.55$, $a = 1.0$, $S_1 = 2.0$, $S_2 = S_3 = 0$

The facesheets are made of a AS4/3501-6 carbon/epoxy fibrous composite laminate, and each consists of eight plies arranged in a quasi-isotropic $(0/\pm 45/90)_s$ symmetric layup. The overall moduli of a unidirectional AS4/3501-6 monolayer are given by Sun and Wu (1991). A classical laminate analysis provided the overall properties of the quasi-isotropic laminate. Resulting values are listed in Table 1, and refer to the material principal axes, which are oriented in direction of the 0° and the 90° fibers. The carbon fiber is assumed to be linearly elastic, but the epoxy matrix may exhibit time dependent deformation. However, elastic response is expected to dominate the behavior of the laminate under high strain rates. Therefore, the facesheets are treated as homogeneous, orthotropic elastic material layers, and defined in the numerical calculations by *LS-Dyna Material Type 2*.

The polyurea interlayer is a rate-sensitive, elastic–plastic material, with properties found in recent high velocity impact experiments (Nemat-Nasser, 2004). This material exhibits stiffening with both increasing strain and strain rate, as described by an elastic–plastic–hydrodynamic model with the Gruneisen equation of state. The material is assumed to be plastically incompressible with pressure dependent yield strength

$$\sigma_y = \sigma_y^o + E_h \bar{\varepsilon}^p + (a_1 + a_2 p)\max[p, 0], \tag{1}$$

where σ_y^o is yield stress of the virgin material, E_h is elastic–plastic tangent modulus of the stress–true strain curve under compression, and $\bar{\varepsilon}^p$ is effective plastic strain. Isotropic hardening due to induced pressure p is given by the last term in Eq. (1), where a_1, a_2 are material parameters.

The material behavior under hydrostatic load, or dilatation caused by shock compression, is described by Gruneisen's equation of state

$$p = \frac{\rho_0 C^2 \mu\left[1 + \left(1 - \frac{1}{2}\gamma_0\right)\mu - \frac{1}{2}a\mu^2\right]}{\left[1 - (S_1 - 1)\mu - S_2\frac{\mu^2}{(1+\mu)} - S_3\frac{\mu^3}{(1+\mu)^2}\right]} + (\gamma_0 + a\mu)e. \tag{2}$$

Here, e is the internal energy per current specific volume and $\mu = (\rho/\rho_0) - 1 = (V_0/V) - 1$ is a measure of dilatation, with ρ_0 and V_0 denoting the initial mass density and volume, and ρ and V their current counterparts. Constants C, S_1, S_2, *and* S_3 are fitting parameters for the shock velocity–particle velocity curve, γ_0 is the Gruneisen gamma, and a is the first order volume correction to γ_0. In the finite element analysis, the polyurea interlayer was represented by *LS-Dyna Material Type 10* and *Equation of State Type 4*.

Table 2 lists the material parameters utilized in Eqs. (1) and (2) for polyurea to qualitatively correlate the computed response with the experimental results given by Nemat-Nasser (2004). Predictions of this material model under strain-controlled compressive loading applied at various rates (Fig. 3) exhibit sensitivity to both strain rate and pressure. Reversing the applied strain causes a sudden reduction in the stress due to unloading of the induced shock pressure, followed by recovery of elastic strains.

The structural foam core material (H100 Divinycell) is an isotropic, closed cell foam. Under uniaxial compression, it deforms as shown Fig. 4 (Fleck, 2004). The response is linearly elastic up to the yield stress of 1.7 MPa, and is followed by perfectly inelastic compression up to 55% of strain. Increasing the strain beyond this magnitude initiates locking, marked by sharply increasing compression load. Incompressible response is reached at the densification strain of approximately 80%. At a small Poisson's ratio, this is essentially a uniaxial crushing model, which follows the stress–strain curve of Fig. 4. In this case, the abscissa represents volumetric strain. Unloading is elastic up to a small tensile cutoff stress. Continued strain-controlled unloading occurs at a constant stress at the tension cutoff magnitude. Reloading is elastic up to a stress and strain pair, which falls on the loading branch of the stress–strain curve. In the finite element calculations, the foam was modeled by *LS-Dyna Material Type 63*.

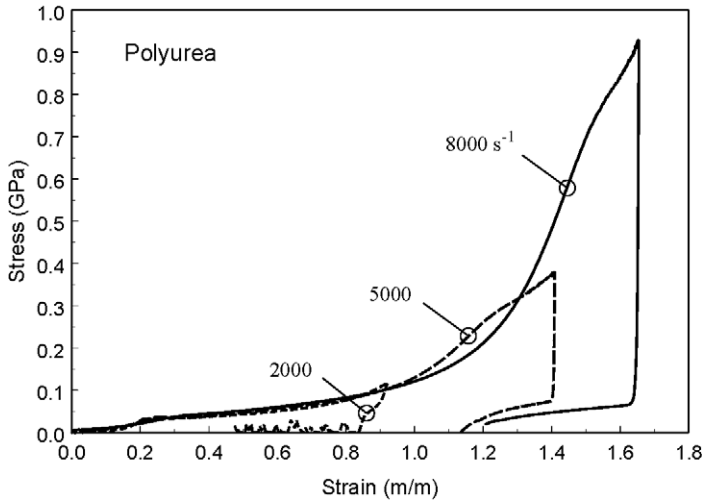

Fig. 3. Stress–strain behavior of polyurea under compression.

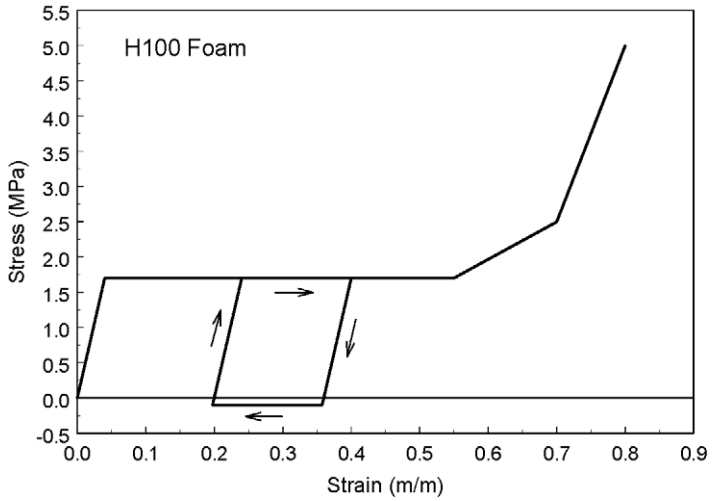

Fig. 4. Stress–strain behavior of H100 closed cell foam under compression.

Delamination of the facesheet from the core is one of the major damage mechanisms in sandwich plates subjected to static and dynamic loads. Our previous work in analysis of sandwich plates subjected to impulse pressure using the finite element method (Dvorak and Bahei-El-Din, 2005) revealed that such delamination cracks occur in the outer, loaded side at the onset of loading, and they propagate through the entire interface in a very short period. Extensive delamination of the inner facesheet also occurs after a short delay. Since both the tensile and shear strength of the foam core are very low, the delamination cracks due to impulse loads are expected to occur in the structural foam along a path adjacent to its interface with the facesheets. In our previous work we have found that modeling progressive delamination in sandwich plates subjected to impulse loads produces the same response given by a fully disjointed interface between the foam and the face layers. In the present analysis all interfaces between the foam core and facesheets, or polyurea interlayer, were kept in contact without cohesion in the stress free state, and allowed to open under tensile traction, and slide relative to each other under shear. Interpenetration was prevented. However, a perfect bond of the outer facesheet to the polyurea interlayer was prescribed in the finite element analysis.

Blast loads caused by explosives induce pressure p on the exposed structural surfaces. They are described by an assumed, exponentially decaying function of time t (Low and Hao, 2001; Gantes and Pnevmatikos, 2004),

$$p(t) = p_{\max}\left(1 - \frac{t}{t_d}\right)e^{-bt/t_d}, \tag{3}$$

where $p_{\max}$ is the peak reflected positive pressure and t_d is the time for pressure reversal. The pressure decay rate is given by the ratio b/t_d. The negative pressure phase of the blast load diminishes for $b \gg 1.0$. Since the negative pressure phase is usually neglected in the analysis of structures subjected to explosives, the magnitude of b was assumed equal to 2.0. Fig. 1b shows the load history of Eq. (3) for peak pressure $p_{\max} = 100$ MPa, and pressure reversal time $t_d = 0.05$ ms. This pressure was applied to the outer facesheet, as shown in Fig. 1c.

If this peak pressure were caused by a spherical TNT explosive charge of weight W (kg) placed at a distance R (m) from the outer surface of the sandwich plate, it could be written in terms of the scaled distance $Z = R/\sqrt[3]{W}$ as the Brode empirical function (Brode, 1955; Low and Hao, 2001)

$$p_{\max}(\text{bar}) = \begin{cases} \dfrac{6.7}{Z^3} + 1 & \text{for } p_{\max} \geqslant 10, \\ \dfrac{0.975}{Z} + \dfrac{1.455}{Z^2} + \dfrac{5.85}{Z^3} - 0.019 & \text{for } 0.1 \leqslant p_{\max} < 10. \end{cases} \tag{4}$$

If r denotes the radius of a spherical explosive charge, then (4) gives the ratio $R/r = 3.5$ at peak pressure $p_{\max} = 100$ MPa. This peak pressure may be caused, for example, by a TNT spherical explosive charge with a radius of 10 cm, and weight of 6.7 kg, placed at a distance equal to 35 cm from the outer surface of the sandwich plate, measured from the center of the explosive charge. Eq. (4) suggests that the magnitude of the positive peak pressure induced by explosives decreases quite rapidly with the distance R. Consequently, the uniform pressure applied in Fig. 1 at the peak value of 100 MPa could be the effect of an array of explosive charges placed at equal distances from the outer surface of the sandwich plate.

3. Finite element models

Response of the two sandwich plate designs shown in Fig. 2 to blast loading was examined using the finite element method. The LS-Dyna software (LSTC, 2003) was used. It performs a Lagrangian dynamic analysis using an explicit, central difference integration scheme. The method is conditionally stable for time increments that are smaller than Courant time limit, $\Delta t \leqslant \ell/c$, where ℓ is the smallest element dimension, $c = \sqrt{(\lambda + 2\mu)/\rho}$ is the speed of sound waves in the medium, λ and μ are Lame's elastic constants, and ρ is the density of the material. Consequently, the solution is advanced at fairly small time increments but it does not involve solution of large simultaneous equations for nodal displacements and as such it is relatively inexpensive. Instead, the nodal accelerations are computed from the nodal forces, which represent in part the applied element pressure (Fig. 1c), and the lumped mass. The nodal accelerations are then used to advance the velocity solution to time $t + \Delta t/2$, which in turn is used to calculate the displacements at time $t + \Delta t$.

The solution domain was selected as a 'unit cell' consisting of a single span that extends over the support on either side, to the middle of the next span, as shown in Fig. 1c. In general, this selection suggests that the plate deformations are symmetric with respect to X_2X_3-planes located at the ends of the unit cell of Fig. 1c. Under a uniform load applied as shown in Fig. 1c, the plate deformations are also symmetric with respect to the X_2X_3-plane located at the center of the middle span. In this case, the solution domain was reduced from that shown in Fig. 1c to one which contains half of the loaded span, and half of the adjacent span, Fig. 5. The pressure load of Fig. 1b was applied as a uniform stress, perpendicular to the exterior surfaces of the outer laminated facesheet elements.

Let u_i, $i = 1, 2, 3$, denote the displacements referred to the overall coordinate system X_i, $i = 1, 2, 3$, shown in Fig. 5. The following boundary conditions were applied to reflect symmetry of the deformations at the center of the plate spans

$$u_1(0, X_2, X_3) = u_1(L, X_2, X_3) = 0, \quad -\infty < X_2 < \infty, \quad 0 \leqslant X_3 \leqslant h. \tag{5}$$

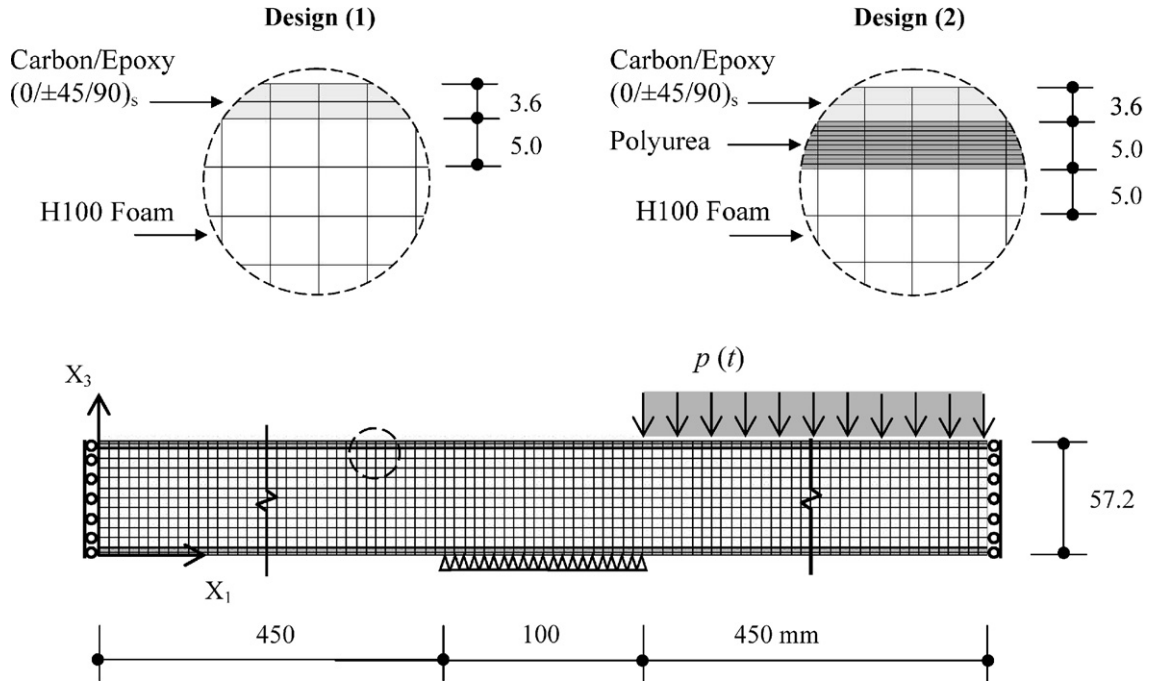

Fig. 5. Finite element solution domain and mesh.

Plane strain in the transverse, X_2, direction of the sandwich plate of Fig. 1, was implemented by the following boundary condition:

$$u_2(X_1, X_2, X_3) = 0, \quad 0 \leqslant X_1 \leqslant L, \quad -\infty < X_2 < \infty, \quad 0 \leqslant X_3 \leqslant h. \tag{6}$$

At the rigid support, the displacement boundary conditions are

$$u_1(X_1, X_2, 0) = u_3(X_1, X_2, 0) = 0, \quad \frac{1}{2}(L-d) \leqslant X_1 \leqslant \frac{1}{2}(L+d), \quad -\infty < X_2 < \infty. \tag{7}$$

Under blast loads induced in direction of the X_3-axis, propagation of transverse stress waves in the X_1-direction slows down dramatically, due to material inhomogeneity and nonlinearity. Hence the transmitted effect of remote load repetitions, implied by the symmetry boundary conditions (5), on response of a particular span will be negligible.

In the finite element mesh of Fig. 5, brick elements of a constant width were utilized. Although the unit cell and loading shown in Fig. 1 suggest a plane strain analysis, the problem was treated as three-dimensional subjected to plane strain boundary conditions, Eq. (6), in order to utilize the LS-Dyna material models indicated in Section 2 One row of brick elements, with a width of 1.0 mm was utilized in the X_2-direction.

The insets in Fig. 5 show details of the mesh for Designs (1) and (2). A uniform mesh was utilized in the longitudinal, X_1-direction in all material parts. The dimension of the brick elements in this direction is 5.0 mm. The element dimension in the thickness direction X_3 varied among the material parts. The mesh through the core thickness consisted of 5.0 mm-thick elements. Since the foam core thickness varied according to the sandwich designs, Fig. 2, the number of core elements in the X_3-direction was 10 in Design (1) and 9 in Design (2). Thickness of the laminated facesheets was modeled with two elements, each is 1.8 mm wide.

A more refined mesh was selected in the polyurea interlayer in Design (2) where 10 elements, each is 0.5 mm wide, were used through the thickness. This enhances resolution of the stress and strain and captures the stiffening effect, which characterizes this material under shock compression.

Delamination of the foam core from either the laminated facesheets or the polyurea interlayer was assumed to occur at the onset of loading, hence the interfaces with the foam were in contact in the unloaded state, and free to move relative to each other under load without interpenetration. This was modeled by introducing

surface to surface contact conditions at the disjointed surfaces. Also, to prevent element deformations into negative volumes, particularly in the crushable H100 foam elements, the LS-Dyna's interior contact capability was activated. Finally, artificial bulk viscosity was activated to properly represent propagation of the induced compression stress waves. Both quadratic and linear functions of the volumetric strain rate were used, and their coefficients were kept constant at 1.5 and 0.06, respectively. In this way, the response of sandwich plates with conventional and modified designs to blast loads is compared on equal footing.

4. Response to a full-span blast pressure

When the blast pressure of Fig. 1b is applied to the entire middle span of the sandwich plate, Fig. 1c, each of the two designs of Fig. 2 undergoes a particular deformation history, which determines the distribution of the kinetic and strain energy absorbed by the different layers of the sandwich structure. This section provides description of the overall and local response of the sandwich plate of Fig. 1 to blast loading.

4.1. Local and overall deformations

The extent of delamination and compression of the foam core, and the overall deformation of the conventional sandwich plate Design (1) and the modified Design (2) are illustrated in Figs. 6 and 7 at $t = 0.25$–5.0 ms, well past the initial loading period of 0.05 ms. The foam core undergoes large compressive or crushing deformation in the top half of the core layer, resulting in substantial thickness reduction of the core thickness.

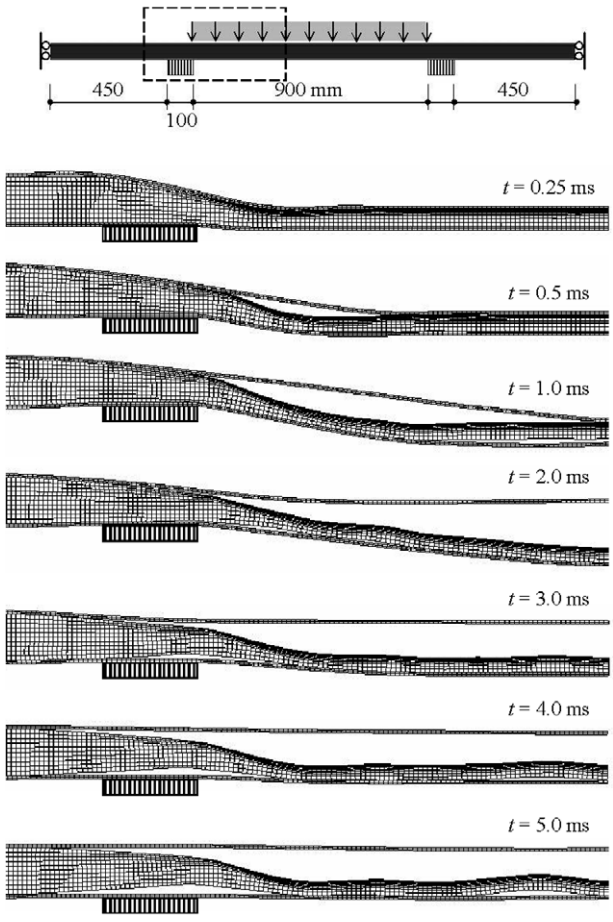

Fig. 6. Deformed geometry of a sandwich plate with conventional Design (1).

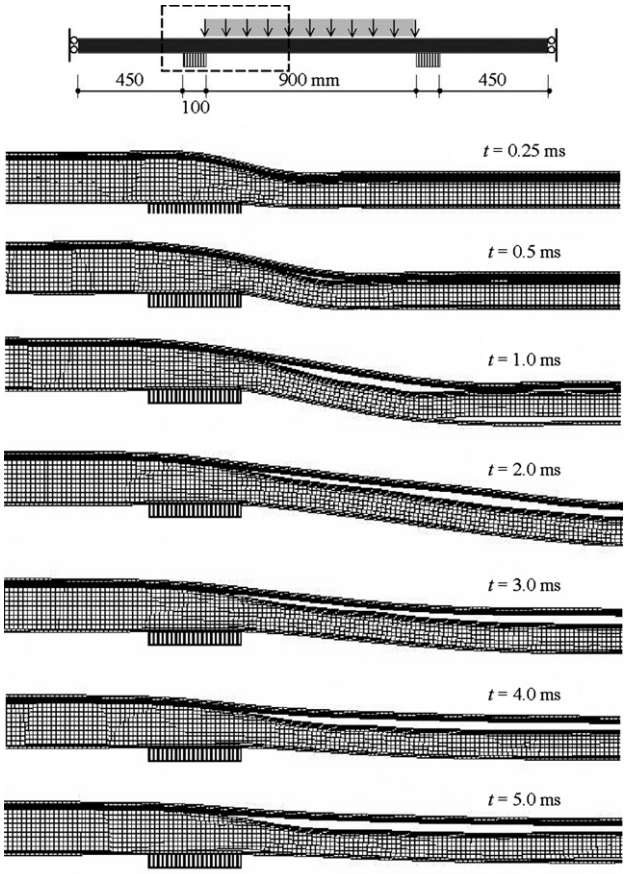

Fig. 7. Deformed geometry of a sandwich plate with enhanced Design (2).

Under the uniformly applied pressure, the foam compression is largest in center of the span, and then decreases in sections that are located closer to supports. Large displacement gradients are present in both the outer and inner facesheets. In the outer facesheet, these are associated with the significant deflections of its surface under the applied pressure. On the other hand, the displacement gradient in the inner facesheet is caused by the constraints imposed by the supports.

Delamination of both outer and inner facesheets from the core was detected, in the form of displacement jumps in both normal and tangential directions to the interfaces, which are initially closed. The latter, sliding separation mode is marked by the misalignment of the finite element mesh at certain closed parts of the facesheet/core interface, as seen in Figs. 6 and 7. Both normal and sliding modes may materialize and interact at a particular interface point during the response time period. The conventional Design (1), Fig. 6, undergoes extensive thinning of the foam core and separation of both the outer and inner facesheets accompanied by large displacement jumps. These deformations are substantially reduced in the modified Design (2), Fig. 7. The deformed geometry of the sandwich plates suggests that core compression is initially the dominant deformation mechanism, followed by bending. The outer and inner facesheets however undergo different bending deformations due to their separation from the foam core, and nonuniform compression of the latter.

An illustration of the evolution of facesheet delamination in the conventional Design (1), and the modified Design (2) of Fig. 2, is shown in Fig. 8 where the normal displacement jump across the facesheet/core interface is plotted as a function of time for the mid-span plate section. The results show a rapid growth of the opening displacement at the debonded outer interface for the conventional Design (1). The peak displacement was reduced almost by a factor of 5 in the modified Design (2). Facesheet separation also occurs at the inner interface in both designs, but it is not as significant as it is at the outer facesheet/core interface.

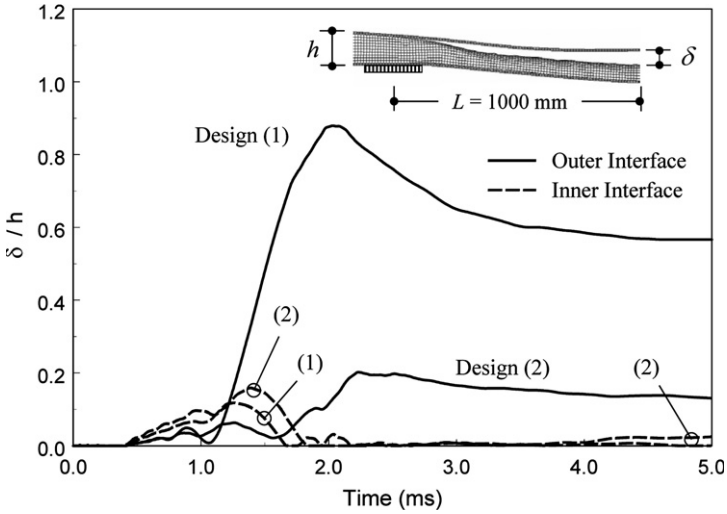

Fig. 8. Facesheet/core interface opening displacement.

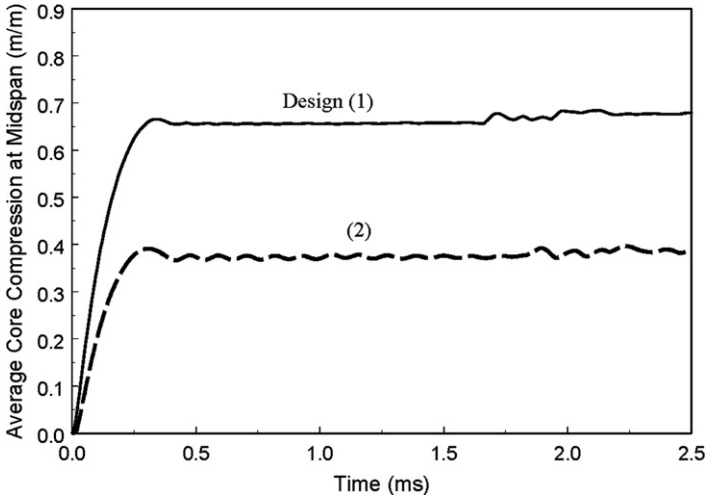

Fig. 9. Average core compression.

Averaged core compression at mid-span, computed as the ratio $\Delta h_c/h_c$, where h_c is thickness of the foam core and Δh_c is the change in its magnitude, is plotted in Fig. 9 as a function of time. A steady state is reached within about 0.3 ms, after a rapid rise to average strains of 0.4–0.68. The stiffening polyurea interlayer found in Design (2) appears to absorb the induced shockwave, and thus better protect the inner foam core from crushing, which is reduced to about 40% of that in Design (1).

While these averages indicate the magnitude of thinning of the sandwich plate cross-section, they are caused by much larger compressive or crushing strains, which are nonuniform across the thickness. Fig. 10 shows distribution of the lateral strain ε_{33} within the foam core thickness at mid-span for Designs (1, 2) at 0.5 ms. At a densification strain of about 0.8, it is evident from the stress–strain response of the H100 foam in Fig. 4 that the foam in Design (1) reaches full densification for the outer 50% of the foam cross-section. On the other hand, only the outer 20% of the core cross-section in Design (2) is fully compressed.

Maximum deflection of the sandwich plates was evaluated as the displacement in the X_3-direction of Fig. 1, of the exterior surfaces of the inner facesheet, $X_3 = 0$, and the outer facesheet, $X_3 = 57.2$ mm, at mid-span, $X_1 = L$. Fig. 11 compares the deflection histories for the two designs. Progressive crushing of the foam core

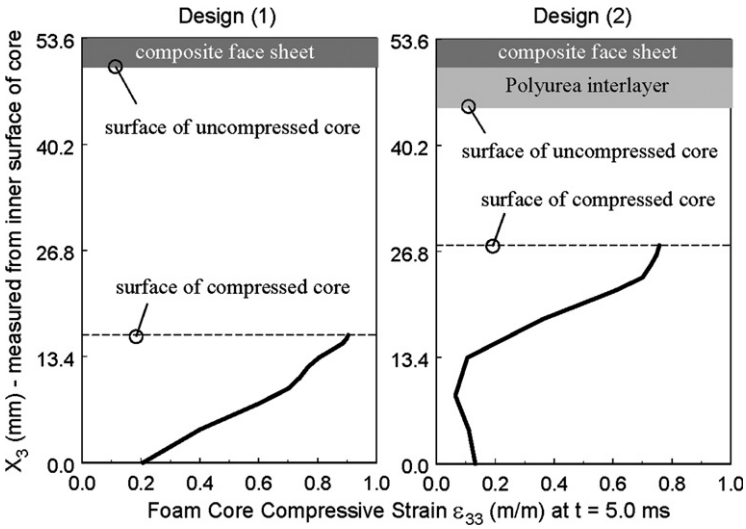

Fig. 10. Strain distribution within the thickness of the foam core.

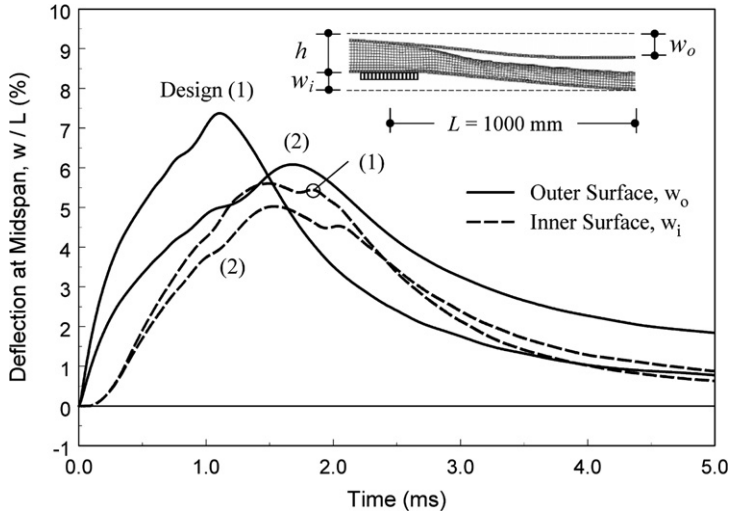

Fig. 11. Mid-span deflection at outer and inner surfaces.

causes the deflections at the outer and the inner surfaces to grow at different rates, which are much higher at the outer surface. The effect of foam core compression on surface deflections is however limited to the initial loading stage, after which bending deformations are dominant. Hence the reduction of the foam core compression achieved in Design (2) compared to Design (1) accounts for a relatively small reduction in overall deflections. As seen from Fig. 11, there is a 20% reduction in deflection of the outer surface of the sandwich plate in the middle of the loaded span when Design (2) with a polyurea interlayer is utilized, and 10% reduction in deflection of the inner surface.

4.2. Facesheet strains

Longitudinal strains computed in the composite facesheets are plotted in Figs. 12 and 13. The values shown for the outer, loaded facesheet in Fig. 12 represent the strain at the interface with the foam core in Design (1), and with the polyurea interlayer in Design (2). For the inner facesheet, the strains shown in Fig. 13 for both

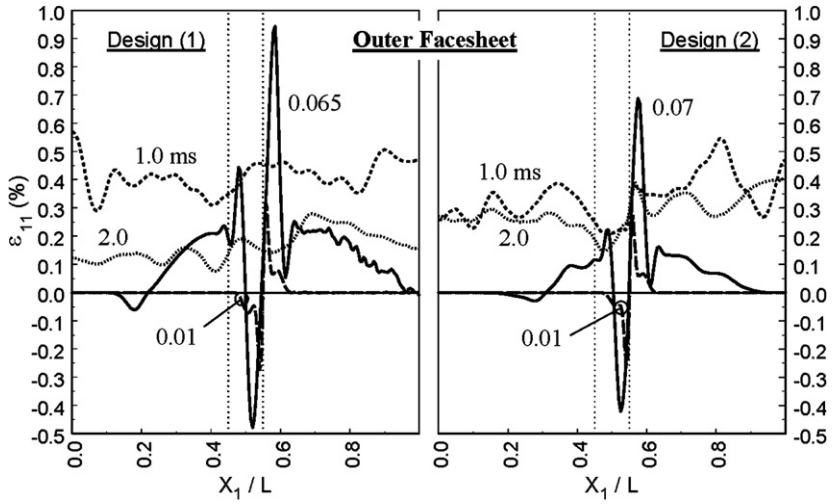

Fig. 12. Distribution of longitudinal strain in the outer facesheet.

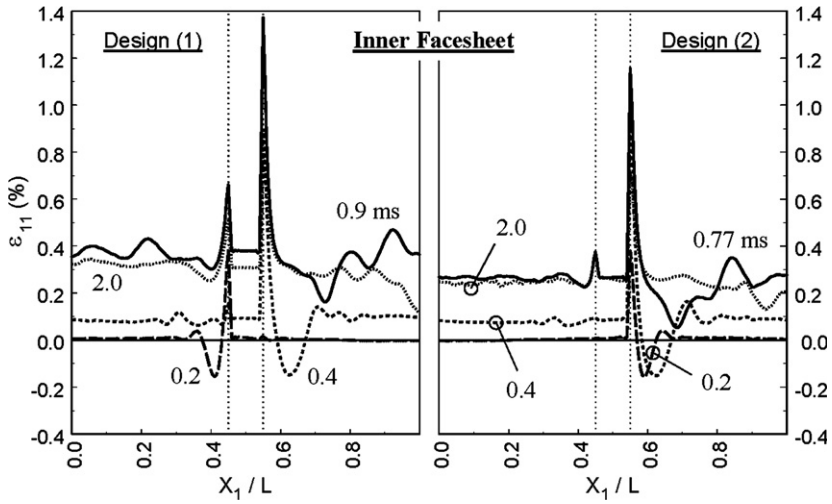

Fig. 13. Distribution of longitudinal strain in the inner facesheet.

designs were found at the interface with the foam core. The plots present the strain distribution in the longitudinal, X_1-direction of the sandwich plates at several time intervals. The two dotted vertical lines located at $X_1/L = 0.45,0.55$ indicate the boundaries of the rigid support. As indicated in Fig. 1c, the pressure load is applied at the center span, or at $0.55 \leqslant X_1/L \leqslant 1.0$ for the solution domain of Fig. 5.

At the onset of blast load of Fig. 1b, the largest longitudinal strain magnitudes occur in both the outer and inner facesheet at the edge of the support on the loaded span side. The maximum tensile strain in the outer facesheet of the conventional Design (1) is 0.0095 and is reduced by 30% to 0.0067 in Design (2) with the polyurea interlayer. In the inner facesheet, Design (2) reduced the peak longitudinal strain by 18%. Since the ultimate longitudinal strain of the carbon/epoxy laminate is controlled by that of the fiber, which is in the order of 1–2% for most carbon fibers, failure under the blast load of Fig. 1b is expected to occur in the inner facesheet, Fig. 13. It is seen however that the enhanced Design (2) may suppress or provide additional safety against this failure mode by reducing the crushed volume of the foam core and hence reducing the curvature at the support. The tensile strains in the outer facesheet in both sandwich designs are below the failure

limit. This is facilitated by separation of the facesheet, and the attached polyurea interlayer, from the foam core, and leads, eventually, to an almost uniform longitudinal strain in the facesheet. On the other hand, the inner facesheet remains in contact with the foam core (Figs. 6 and 7), and undergoes permanent bending and stretching. By protecting the foam core with the polyurea interlayer, these effects have been reduced substantially in Design (2).

4.3. Energy absorption

The total energy imparted by the applied pressure impulse to the sandwich plate parts is converted to kinetic and strain energy. The latter is either dissipated by inelastic deformation and damage, or stored by the elastic material parts. The elastic strain energy is stored primarily in the outer and inner composite facesheets. Energy dissipation occurs in the crushable foam core, and in the elastic–plastic polyurea interlayer in Design (2). The reported energy magnitudes refer to the total volume of each layer. We note that the volume ratio of the outer facesheet to the foam core is 7% in Design (1) and 8% in Design (2). The volume ratio of the polyurea interlayer to the foam core in Design (2) is 11%.

Fig. 14 shows time histories of the kinetic energy of the individual layers of the sandwich plate Designs (1) and (2). The kinetic energy is initially imparted to the outer composite facesheet by the applied load. The induced compression wave propagates into the underlying materials, with particle velocity affected by the material properties. In Design (1), the facesheet is supported by the foam core, which exhibits permanent crushing under a small compressive stress. Therefore, the total kinetic energy in this design is mostly imparted to the outer facesheet at a peak value of 60 J. This is reduced by a factor of 1.7 in Design (2), where the kinetic energy resides in the outer facesheet and polyurea materials. The implication is that in the presence of the stiffening polyurea interlayer, the facesheet of Design (2) sustains smaller velocities and hence less kinetic energy.

Distribution of strain energy among the sandwich plate material parts is shown in Fig. 15. In either design, the energy absorbed by the elastic composite facesheets is small, and is eventually recovered. Most of the strain energy of the sandwich plates is dissipated by permanent deformations of the foam core in both designs, and of the polyurea interlayer in Design (2). In Design (1), the energy dissipated by crushing of the entire volume of the foam core is 40 J. In the enhanced Design (2), both crushing of the foam core and plastic deformation of the polyurea account for the total dissipated energy of 25 J; a reduction of about 38% from that found in Design (1).

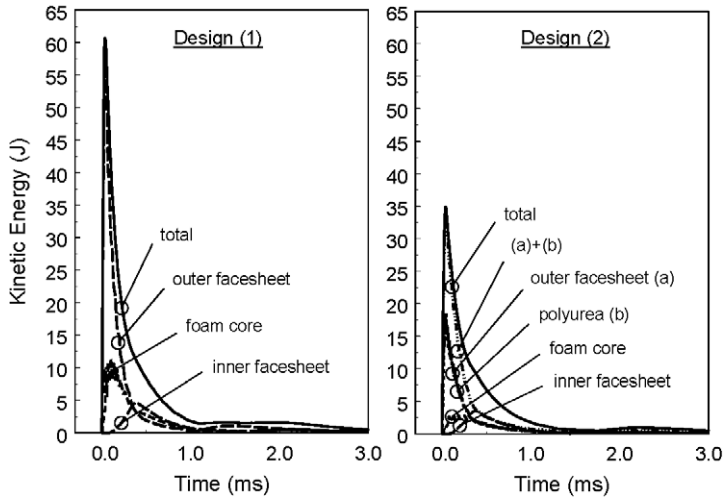

Fig. 14. Distribution of kinetic energy.

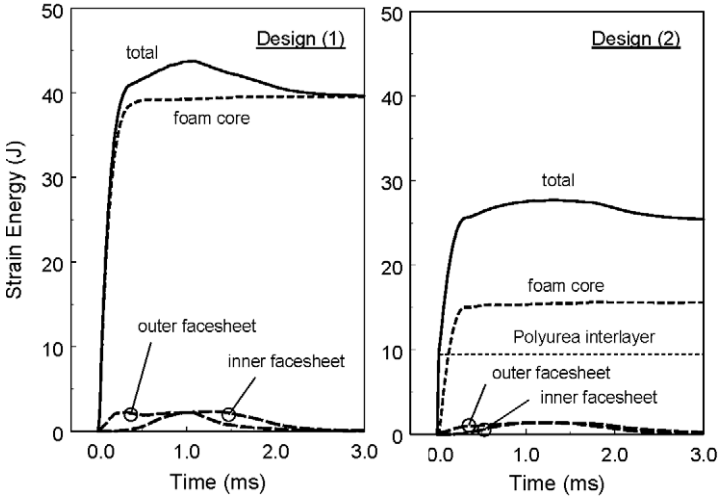

Fig. 15. Distribution of strain energy.

5. Discussion and conclusions

The results show that the proposed modification of sandwich plate design provides superior performance under blast loads, both during the initial response period that is characterized by crushing of the foam core, and during the bending and stretching phase. The much more graceful response found in the modified design of a continuous sandwich plate subjected to a full span blast load is attributed to the stiffness increase caused by straining a polyurea interlayer, which separates the facesheet and the foam core, at high rates. This protects the foam core from excessive crushing, and also reduces vibrations of the facesheet and overall deflection of the plate. As a result, the total kinetic energy of the modified sandwich plate is much lower than that of a conventionally designed plate. Similar reductions are found in the stored and dissipated strain energy. A large part of the reduced strain energy is absorbed by the polyurea interlayer, where it is dissipated by inelastic deformation.

Other important benefits from the ductile polyurea interlayer utilized between the facesheet and the foam core include significant reductions in the facesheet strains, the plate deflections, and the interface opening between the facesheet and the foam core.

While this study compares the response of conventional (Design 1) and modified (Design 2) sandwich plates to blast loads, the overall dimensions of all plates were not altered, including the total thickness. This results in an increase of 30% in the total mass of the conventional Design (1) when the top 5 mm of the inner foam core is replaced with a polyurea interlayer of equal thickness in Design (2), Table 1. Whether the improvements found in response of the sandwich Design (2) under blast loads can be realized while the total mass of the plates is kept constant was examined by modifying the thickness of the foam core. Since it is not possible to achieve equal mass in the two designs examined here (Fig. 2) by reducing the thickness of the modified Design (2), the thickness of the foam core in the conventional Design (1) was instead increased from 50.0 to 98.5 mm. In this case, the total thickness of the plate in Design (1) is 105.7 mm compared to 57.2 mm in Design (2), and the mass per unit surface area for each plate is 21.23 kg/m^2.

The enhanced Design (2) with a polyurea interlayer continues to show a significant improvement in response to blast load compared to the conventional sandwich Design (1) of equal mass. The total, peak kinetic energy was reduced by 43%, and energy dissipation in the entire volume of the foam core was reduced by 38%. These reductions are equal to those found when the standard and modified sandwich plates have equal thickness. The implication is that a smaller volume of the foam core is permanently compressed when a polyurea interlayer is used. Also, the ratio (δ/L), between the facesheet/core interface opening and the core thickness in the modified Design (2) is 0.1 compared to 0.55 in Design (1), which has equal mass. On the other hand, the large thickness of the conventional sandwich plate with mass equal to that of the modified design

leads as expected to smaller bending deformations. In this case, the maximum tensile strain in the inner composite facesheet at the support for the conventional sandwich plate was computed at 1%.

Acknowledgements

The authors gratefully acknowledge the support provided by the Office of Naval Research. Dr. Yapa D.S. Rajapakse served as program monitor.

References

Brode, H.L., 1955. Numerical solution of spherical blast waves. Journal of Applied Physics 26 (6), 766–775.

Clifton, R., Jiao, T., 2004. High strain response of elastomers. In: Proceedings of ONR, ERC, ACTD Workshop, MIT, Cambridge, Massachusetts, November 2004.

Dvorak, G.J., Bahei-El-Din, Y.A., 2005. Enhancement of blast resistance of sandwich plates. In: Proceedings of the 7th International Conference on Sandwich Structures, 29–31 August 2005. Aalborg University, Aalborg, Denmark.

Dvorak, G.J., Suvorov, A.P., 2006. Protection of sandwich plates from low-velocity impact. Journal of Composite Materials (in press).

Fleck, N.A., 2004. Collapse mechanisms of sandwich beams with composite faces and foam core, loaded in three-point bending. Part II: experimental investigation and numerical modeling. International Journal of Mechanical Sciences 46, 585–608.

Fleck, N.A., Deshpande, V.S., 2004. The resistance of clamped sandwich beams to shock loading. ASME Journal of Applied Mechanics 71, 386–401.

Florence, A.L., 1966. Clamped circular rigid-plastic plates under blast loading. ASME Journal of Applied Mechanics 33, 256–260.

Gantes, C.J., Pnevmatikos, N.G., 2004. Elastic–plastic response spectra for exponential blast loading. International Journal of Impact Engineering 30, 323–343.

Jones, N., 1971. A theoretical study of the dynamic plastic behaviour of beams and plates with finite deflections. International Journal of Solids and Structures 7, 1007–1029.

Jones, N., 1989. Structural Impact. Cambridge University Press.

Low, H.Y., Hao, H., 2001. Reliability analysis of reinforced concrete slabs under explosive loading. Structural Safety 23, 157–178.

LSTC, 2003. LS-Dyna 970. Livermore Software Technology Corporation, Livermore, CA.

Nemat-Nasser, S., 2004. Experimental characterization of polyurea with constitutive modeling and simulation. In: Proceedings of ONR, ERC, ACTD Workshop, MIT, Cambridge, Massachusetts, November 2004.

Qui, X., Deshpande, V.S., Fleck, N.A., 2003. Finite element analysis of the dynamic response of clamped sandwich beams subjected to shock loading. European Journal of Mechanics A/Solids 22, 801–814.

Sun, C.T., Wu, C.L., 1991. Low velocity impact of composite sandwich panels. In: Proceedings of 32nd AIAA/ASME/ASCE Structures, Structural Dynamics and Materials Conference, pp. 1123–1129.

Suvorov, A.P., Dvorak, G.J., 2005a. Enhancement of low-velocity impact resistance of sandwich plates. International Journal of Solids and Structures 42, 2323–2344.

Suvorov, A.P., Dvorak, G.J., 2005b. Dynamic response of sandwich plates to medium-velocity impact. Journal of Sandwich Structures and Materials 7 (5), 395–412.

Symonds, P.S., Wierzbicki, T., 1979. Membrane mode solutions for impulsively loaded circular plates. ASME Journal of Applied Mechanics 46, 58–64.

Taylor, G.I., 1963. The pressure and impulse of submarine explosion waves on plates. The Scientific Papers of G.I. Taylor, vol. III. Cambridge University Press, Cambridge, UK, pp. 287–303.

Wang, A.J., Hopkins, H.G., 1954. On the plastic deformation of built-in circular plates under impulsive load. Journal of the Mechanics and Physics of Solids 3, 22–37.

Xue, Z., Hutchinson, J.W., 2003. Preliminary assessment of sandwich plates subject to blast loads. International Journal of Mechanical Sciences 45, 687–705.

Xue, Z., Hutchinson, J.W., 2004. A comparative study of impulse-resistant metal sandwich plates. International Journal of Impact Engineering 30, 1283–1305.

Yi, J., Boyce, M.C., 2004. Stress–strain behavior of polyurea and polyurethane: preliminary experiments and modeling results. In: Proceedings of ONR, ERC, ACTD Workshop, MIT, Cambridge, Massachusetts, November 2004.